

Influence of feeding condition on crusher performance and fatigue life

Magnus Evertsson¹, Johannes Quist², Adam Bilock³, Klas Jareteg³

¹ Chalmers University of Technology, dep. Industrial & Materials Science, Gothenburg, Sweden, magnus.evertsson@chalmers.se

² Fraunhofer-Chalmers Centre for Industrial Mathematics, dep. Computational Engineering & Design Gothenburg, Sweden, johannes.quist@fcc.chalmers.se

³ IPS Particle Technology AB, Gothenburg, Sweden

Abstract

The fatigue life and liner wear rate of cone crushers depend on the feeding conditions. Uneven and segregated feed results in unnecessary high force amplitudes that are deleterious for the machine as well as for crusher performance and efficiency.

In this paper, a multidisciplinary approach and methodology are presented to estimate the fatigue life of crusher components and thus the service life of the crusher. We use a bonded dilated polyhedral element model to simulate the particle fracture for nominal and segregated feeding conditions. The resulting forces and stresses are spectra that vary over time. The critical components service life is evaluated by applying fatigue theory combined with the Palmgren-Miner rule for damage.

The results demonstrate the dependency between the feeding condition and the fatigue life expectancy. By addressing the feeding conditions significant unwanted costs for crusher operation and maintenance can be avoided and at the same time, the process performance is improved in terms of a smaller particle size distribution can be achieved.

Keywords: DEM, cone crusher, comminution, fracture, damage cumulation, fatigue failure

Introduction

The cone crusher is one of the most used crushing equipment in mining and aggregate industry globally. A schematic illustration of two types of cone crushers can be seen in Figure 1. The operation of the cone crusher is based on an inner mantle that moves according to an eccentric precession motion allowing for particles to be crushed between the mantle surface and the fixed concave surface. The precession motion is typically controlled by a fixed eccentric throw and frequency. The smallest distance in the lower end of the crusher chamber is called the Close Side Setting (CSS) which also normally controls the product size distribution top size.

The performance and operational quality of a cone crusher process are highly influenced by the feeding conditions. The feeding condition may be described in terms of three main aspects; the amount of material in the chamber/hopper typically referred to as choked or trickle-fed condition, the evenness of the mass concentration around the circumference typically referred to as feed alignment, and finally the size segregation around the circumference. As an example, a cone crusher that is trickle fed with different amounts of mass and size distribution on either side due to segregation will operate completely differently from a choke-fed, ideally aligned and non-segregated feed.

Poor feeding conditions are known to cause pre-mature failure of critical parts such as the main shaft, pinion drive shaft, bearings and so forth. Apart from decisions made in the design and manufacturing

phase of these parts, differences in the load case scenario can be the reason for premature failure. In cases of poor feeding conditions as described above, the forces acting on the crushing surfaces will be periodic with an overlaid variance. The signal displays both features of the fracture of individual rocks, as well as bulk aspects related to where the bulk material is present. If there is an unevenness in the mass concentration or size distribution of bulk material in the crushing chamber, naturally the forces will vary accordingly.

The increased loads lead to increased mechanical stresses. As a cone crusher is a type of machine with a cyclically operating duty cycle due to its rotational motion and because of the large number of repeated cycles, it may therefore also be subjected to fatigue failure. These aspects have been well-known from the field and experimental measurements as well as previous simulation studies [1, 2]. However, advanced discrete element simulations including true fracture models have not yet been used to investigate the relationship between feeding conditions and the forces acting on the machine.

In this paper we propose a novel approach where DEM with a bonded dilated polyhedrons with a cohesive zone model is used to model the breakage process in a Hydrocone type cone crusher in order to predict load and stress variations which in turn can lead fatigue failure.

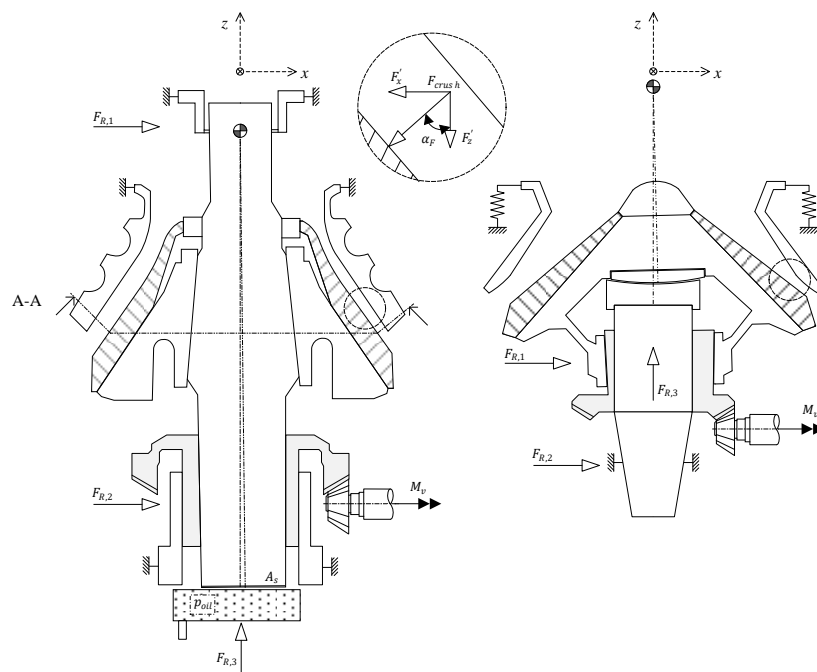


Figure 1. Schematic illustrations of the vertical cross-sections of the Hydrocone (left) and Symons (right) type cone crusher. A simplified representation of the forces can also be seen. Note the difference in pivot point position due to the different mechanical setups.

Method

Cohesive crack zone polyhedral element model

Several approaches have been suggested and implemented for describing particle breakage in the Discrete Element Method (DEM) [3] [4]. The methods may be classified into the algorithms where progeny fragments are resolved from start to end of the simulation, and the algorithms where fragments appear when a critical condition has been met. The first group is usually realized by bonding together spheres as in the Bonded-Particle Model (BPM) [5] or polyhedral cells as in the Bonded Cell Model (BCM) (or FDEM approach) [6] [7] [8] [9]. The latter group of approaches is normally called fragment- or particle replacement methods (PRM). Attempts have been made to use the BPM for full-scale

systems, but while the results were promising, a large enough particle system was not achievable [10, 11]. The PRM is more computationally efficient and has shown promising results [12] [13] [14].

In this work, a fracture model for dilated polyhedral elements has been implemented in Demify® [15], based on Liu [7] and Ma [8, 9]. In the model, adjacent surfaces are bonded by means of damped springs, acting in the normal and shear directions, at each pair of adjacent nodes. When a bond experiences stress fulfilling a Mohr-Coloumb fracture criterion, the bond is damaged. The level of accumulated damage is further on controlled by a cohesive crack zone model where the stiffness of the bond is controlled by the strain energy release rate in mixed mode I and II. If the accumulated damage of a bond exceeds a given threshold, the bond breaks.

The initial particles are modelled based on 3D laser-scanned rocks. The rock mesh convex hull is calculated, and a tetrahedral volume mesh is defined (here using the software gmsh). Particles are entered into the simulation based on a conventional DEM simulation in Demify®. The particles are converted to breakable particles with the mesh representation according to a spatial or time-triggered constraint. The spatial constraint could be e.g., the crushing chamber of a cone crushing as in this work.

Fracture model calibration

The calibration of the fracture model has been conducted based on the diametral compression of a disc, i.e., the Brazilian indirect tensile strength test. In Figure 2 the comparison between the calibrated model parameters is plotted together with different experimental results for granite and diabase. In order to evaluate if the breakage model is temporally convergent the results were evaluated for different time-steps. While there is some variance the results suggest that a shorter time-step successively gives a lower relative error.

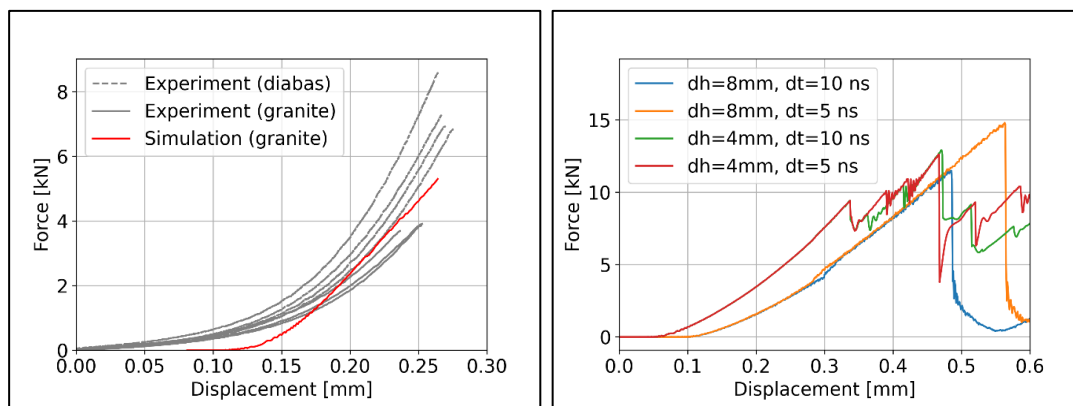


Figure 2. Left: Comparison between Brazilian tensile strength force-displacement for experiment and simulation. Right: Temporal convergence for integration time-step dt and mesh element mean size dh .

Two cone crusher feed case scenarios

Two cases have been defined to evaluate the relationship between feeding condition and probability of fatigue failure for some internal mechanical part. In case 1 a crusher is fed on only one side representing a very common condition normally seen in industrial operations. In the second case the crusher is fed evenly around the circumference, however with twice as much feed mass rate. An illustration of the two case setups can be seen in Figure 3 below.

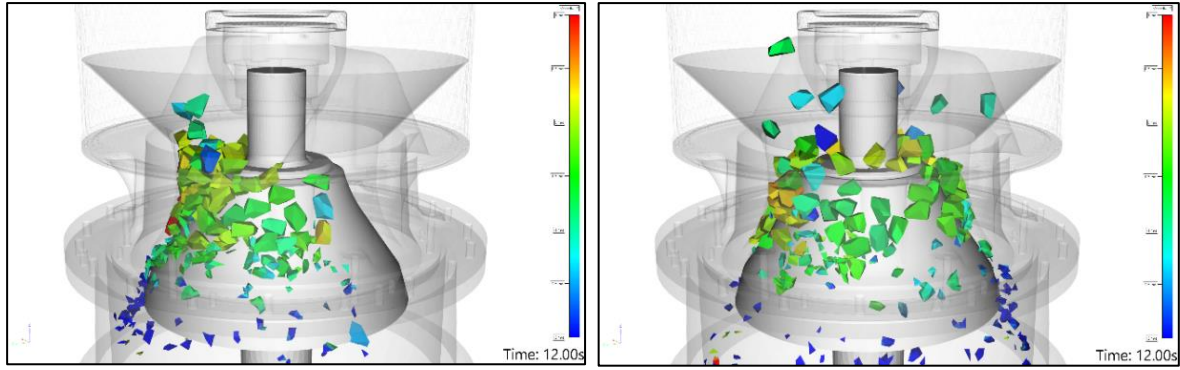


Figure 3. Illustration of the DEM modelling setup of the Hydrocone cone crusher for poor feeding condition to the left and even feeding conditions to the right.

The parameters for the polyhedron element model are presented in Table 1 and the DEM simulation settings in Table 2. The system has been evaluated in terms of time-step convergence however details are omitted for brevity. In general, it is worth mentioning that the performance of the implementation is not demonstrated in this work when it comes to total number of rock particles or elements in the simulation. A rather coarse setup of the element mesh was chosen where the average element size is about half the CSS. For simplicity in this initial study, the feed size distribution was defined as a mono size of 100mm.

Table 1. Bonded polyhedron element model parameters

Parameter	Notation	Value	Unit
Normal strength	$\bar{\sigma}$	6	MPa
Internal cohesion	C	30	MPa
Internal friction	μ_b	0.3	-
Sliding friction p-p	μ_s	0.3	
Strain energy release rate – Mode I	G_I^c	200	J/m ²
Strain energy release rate – Mode II	G_{II}^c	865	J/m ²
Viscous damping coefficient	β	1e-5	-
Young's Modulus Bond	E_b	0.26	GPa
Young's Modulus Rock	E_g	76	GPa
Density	ρ	2700	Kg/m ³
Dilation radius	r_d	0.5	mm
Relative average mesh element size	l_e	0.22	m/m
Number of elements per particle	n_b	123	-

Table 2. DEM simulation settings

Parameter	Notation	Value	Unit
Time-step	dt	5e-7	s
Clock time / sim sec	-	[63,67]	Min / s
GPU	-	RTX 3090	-
Total number of rock particles	N_p	[8610,17220]	-
Sampling frequency	f_s	500	Hz

Table 3. Cone crusher model setup parameters

Parameter	Notation	Value	Unit
Close side setting	CSS	48	mm
Eccentric throw	s_{ecc}	28	mm
Eccentric speed	n_{ecc}	290	rpm
Concave chamber	-	Coarse	-
Feed mass flow	\dot{m}_f	[16, 32]	Kg/s
Feed particle size	x_f	100	Mm

Fatigue life prediction of mechanical components

If a mechanical component is subjected to a time varying load, there is an increasing probability for fatigue fracture with increasing load level. The relationship between the load level and the number of loading cycles can be illustrated in a so called Wöhler diagram (S,N -diagram), see Figure 4. The Wöhler curve can be determined empirically by conducting tests on a large number of specimens at different load levels. The loading cycle is repeated until fracture or failure of the specimen is determined. Because of the statistical variation and spread, several tests must be conducted on each load level.

It is common that components and structures made of steel and its alloys are considered to have an asymptote which in practice is assumed to be valid at 10 million loading cycles ($N = 10^7$). Other material types may in some cases exhibit this type of behaviour. For light metal alloys the asymptotic behaviour is vague but still in practise the fatigue limit is considered to be the stress level corresponding to 100 million loading cycles.

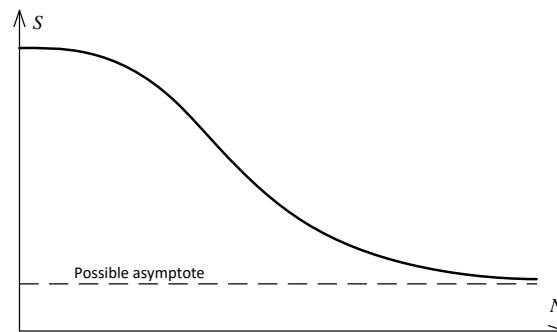


Figure 4. Typical fatigue life in cycles for a mechanical component or part subjected to a varying load.

If the Wöhler curve described with the number of loading cycles to fracture is drawn in a double logarithmic diagram it commonly shows that parts of the curve are close to linear, see Figure 5. The linear part is typically in the interval 1000 to 1000.000 cycles. In this region the failure is characterized by crack initiation and crack propagation and defined as High Cycle Fatigue (HCF). The slope of the linear part of the Wöhler curve defines the fatigue life exponent Basquin's equation, see equation (1).

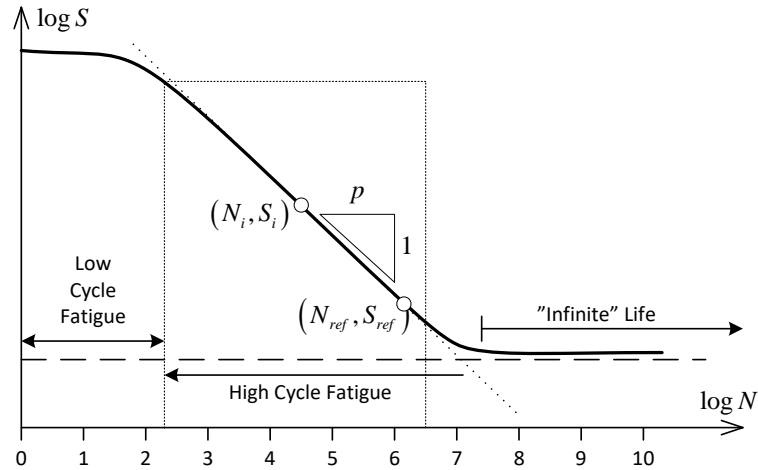


Figure 5. Fatigue life of a mechanical component shown as a $\log S$ - $\log N$ -diagram. The High Cycle Fatigue region appears to be close to linear in this diagram and follows Basquin's equation.

$$N_i = N_{ref} \left(\frac{S_i}{S_{ref}} \right)^{-p} \quad (1)$$

The fatigue behavior of steel structures is described in the European Standard EN 1993-1-9 [16] which is commonly called Eurocode 3 or EC3. In this standard methods are given for assessment of the fatigue resistance of components and structures that are subjected to loads that are varying over time (i.e. fatigue loading). The methods are based on tests with large-scale components and take different effects (geometrical and material imperfections) into consideration. The methods are applicable to all types and grades of steel. Normal operating conditions are assumed (normal atmospheric conditions, no corrosion, no microstructural damage due to high temperatures).

The fatigue strength for nominal stress ranges can be represented in a S, N -diagram which basically shows the relation between the nominal stress range, $\Delta\sigma_R$, and the number of cycles, N , that the material can be subjected to before failure occurs.

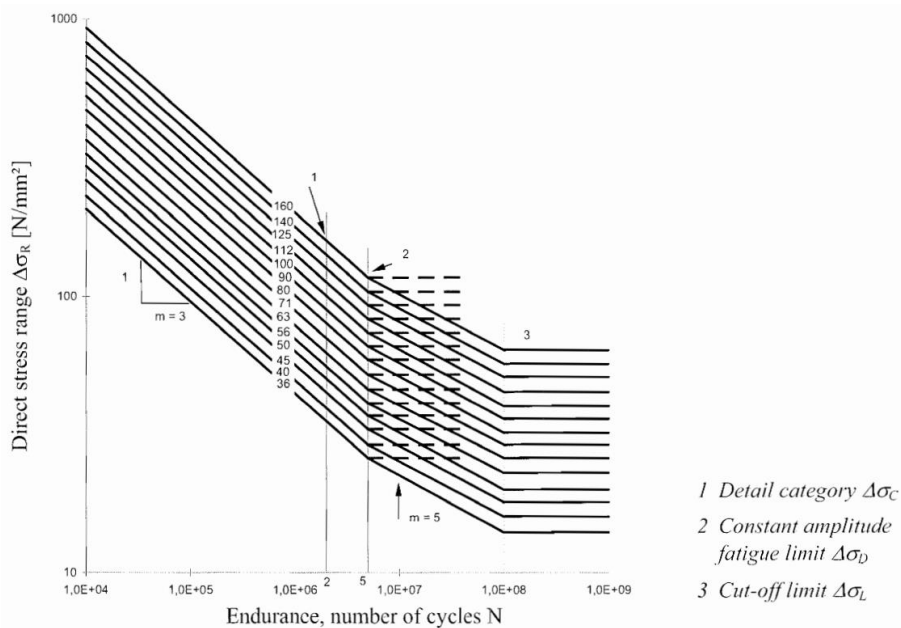


Figure 6. Fatigue strength curves for direct stress ranges according to EN 1993-1-9.

According to EC3, there are several different detail categories which correspond to different material grades. For constant amplitude stress ranges with stress ranges the fatigue strength curve should be composed of two parts:

$$\Delta\sigma_R^m N_R = \Delta\sigma_C^m \cdot (2 \cdot 10^6) \text{ with } m = 3 \text{ for } N \leq 5 \cdot 10^6$$

The reference value of the fatigue strength, $\Delta\sigma_C$, is the stress range corresponding to a fatigue life of 2 million cycles. The constant amplitude fatigue limit $\Delta\sigma_D$ is given by:

$$\Delta\sigma_D = \left(\frac{2}{5}\right)^{1/3} \Delta\sigma_C = 0.737\Delta\sigma_C$$

For nominal stress spectra (i.e. a combination of several different amplitudes) with stress ranges above and below the fatigue limit $\Delta\sigma_D$ each fatigue strength curve should be composed of three parts;

$$\Delta\sigma_R^m N_R = \Delta\sigma_C^m \cdot (2 \cdot 10^6) \text{ with } m = 3 \text{ for } N \leq 5 \cdot 10^6$$

$$\Delta\sigma_R^m N_R = \Delta\sigma_C^m \cdot (5 \cdot 10^6) \text{ with } m = 5 \text{ for } 5 \cdot 10^6 \leq N \leq 10^8$$

The cut off fatigue limit $\Delta\sigma_C$ under these conditions is given by:

$$\Delta\sigma_L = \left(\frac{5}{100}\right)^{1/3} \Delta\sigma_D = 0.549\Delta\sigma_D = 0.405\Delta\sigma_C$$

According to EC3, when test data were used to determine the value of the stress range $\Delta\sigma_C$ corresponding to $N_C = 2 \cdot 10^6$ loading cycles a 75% confidence level for 95% probability of survival were considered.

Cycle Counting in Fatigue Analysis

Cycle counting is a standard practice for handling and summarize (often lengthy) irregular load-versus-time histories by providing the number of times cycles of various sizes occur. Cycle counts can be made for time histories of force, stress, strain, torque, acceleration, deflection, or other loading parameters of interest (ASTM E1049-85, 2017) [17]. In this paper a so-called rainflow counting algorithm based on ASTM E1049-85 is applied. The algorithm uses the original stress variation spectra and identifies the extreme values which in turn is transformed to a time series of reversals. The reversals are then used for the cycle counting and sorted into bins which results in a histogram for the stress amplitude variations.

The Palmgren-Miner Linear Damage Hypothesis

It is reasonable to believe that a structure that is subjected to varying cyclic loading will accumulate damage. The most popular approach for calculating cumulative damage is the Miner's rule which is commonly called the Palmgren-Miners linear damage hypothesis [18] [19].

The hypothesis states that the accumulated damage is the sum of the relative consumption of available life at each stress level.

$$D = \sum_i \frac{n_i(\sigma_i)}{N_i(\sigma_i)}$$

According to the Palmgren-Miners rule failure occurs when the sum reaches the value 1 which means that the total available life of the component is consumed. If a load or stress spectra results in a total damage that is less than 1 then the spectra can be repeated until the damage reaches the value 1.

Results

The simulation results for the two feed cases are shown in Figure 7. It can be seen in the full feed case that some material is lacking on the front view side of the chamber in the image. The reason is due to the top bearing spider arms that to some degree restricts material to flow evenly under the arms. At the feed rates chosen the crushers may be defined as trickle fed and not choke fed. The trickle fed condition was chosen in order to facilitate the evaluation of the feeding on only one side in case 1. If a higher feed rate is chosen, the crusher chamber will eventually fill up and no steady state of case 1 will be seen.

In Figure 8 a more detailed view of a fracture event is displayed with and without mesh elements visualized as dilated polyhedra or polyhedra. The particle in the centre of the image has just experience a body fracture event and the progeny particles are moving away from the event location.

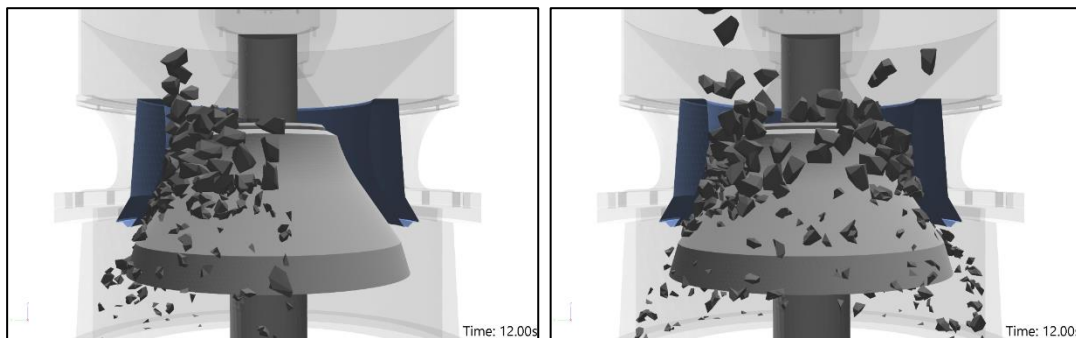


Figure 7. Left: Snapshot from simulation of case 1 - misaligned half feed.
Right: Snapshot from simulation of case 2 - full feed

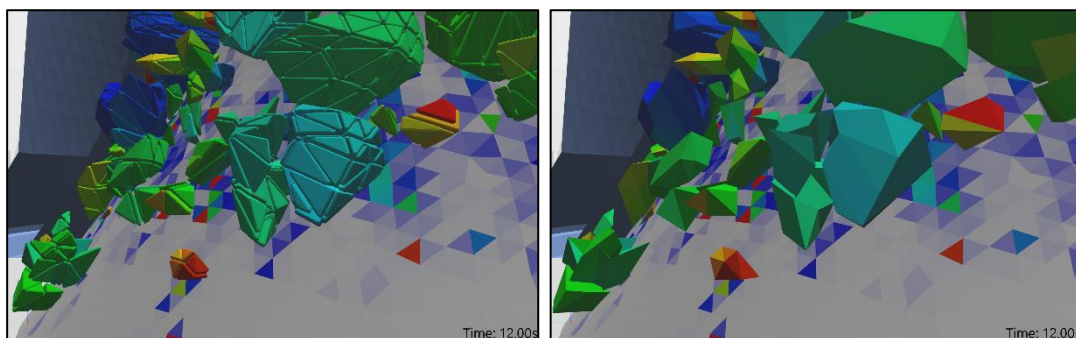


Figure 8. Detailed view of the particles in the crushing chamber. The left image shows the elements including visualization of the dilation radius of each element. The right image displays the particles as polyhedral elements without the dilation radius representation. Particles are coloured according to the velocity norm and the mantle mesh is coloured according to cumulative wear according to Archard's law.

In order to demonstrate how the DEM with fracture can be used to evaluate fatigue failure condition, the main shaft was chosen as a part for study. It is known in industry that the main shaft may have premature fatigue failure that occurs under the crusher head. The forces and moments acting on the mantle surface was sampled for the 12 seconds of simulated operation. The stress in the cross-section of the main shaft under the mantle seating was calculated based on basic machine elements and solid mechanics theory. In Figure 9, the estimated stress magnitude over time is plotted for the two cases. For the half-feed case a cyclic pattern can be seen where the stress varies periodically from zero to a

peak value. This cyclic pattern corresponds to the eccentric speed of the mantle with is 4.82 Hz (290rpm). In the plot to the right the power spectrum plot also reveals a peak at the eccentric frequency of the machine. For the full feed case the stress-time curve instead fluctuates around a mean value with an amplitude. The power spectrum plot does not show the same distinct peak at 4.82 Hz. The scalogram plots in Figure 10 further highlight the 4.82Hz frequency while not distinguishable in the full feed case.

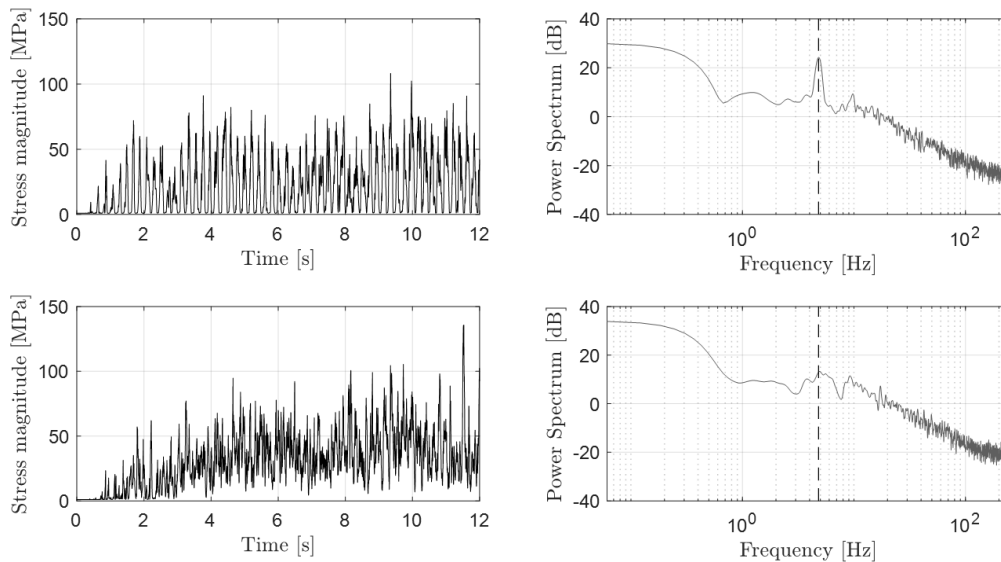


Figure 9. Stress-time signal and power spectrum for the two cases (upper: misaligned feed, lower: full feed). The dashed vertical line represents the eccentric speed of the crusher.

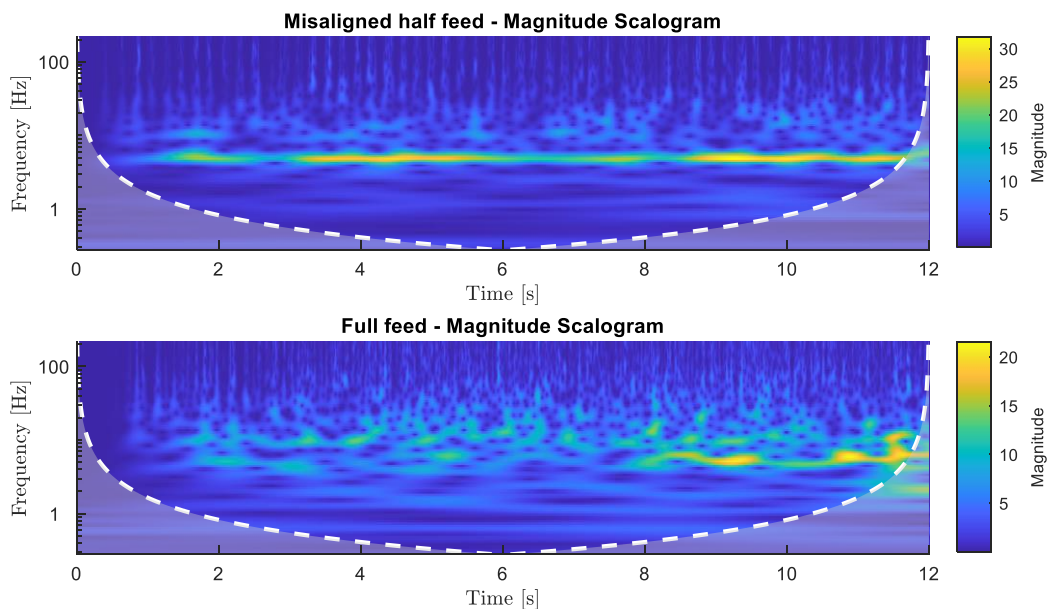


Figure 10. Scalogram for the two cases (upper: misaligned feed, lower: full feed).

To evaluate the relationship between the feeding condition on the potential fatigue failure of the main shaft fatigue strength curves are plotted below according to EN 1993-1-9. The stress signals were analysed using the rainflow counting method according to ASTM E1049-85. This results in a histogram of stress ranges and corresponding counts in each range for the 12 seconds of operation. In Figure 11 the resulting S-N fatigue strength curves are presented if considering one year of continuous

operation. The two cases are relatively close and the damage parameter according to Palmgren-Miner is slightly higher for the full feed case.

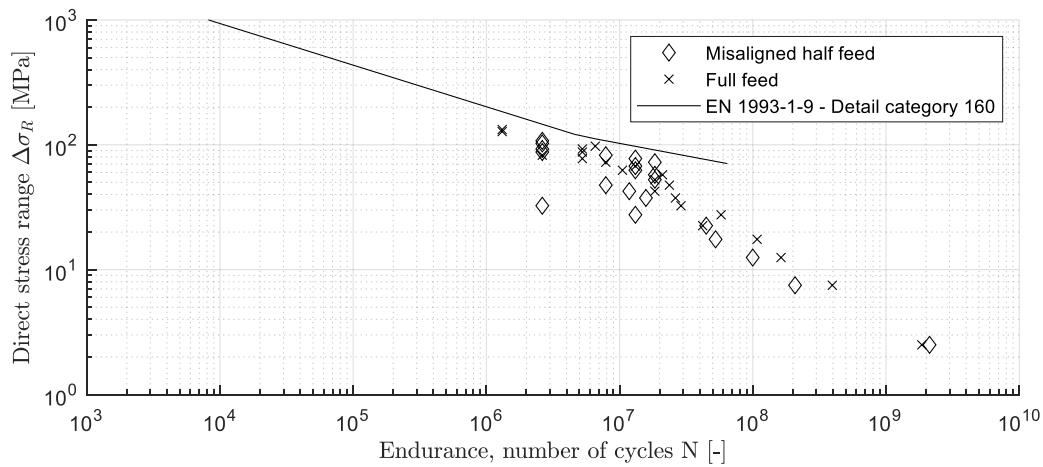


Figure 11. Fatigue strength curves (direct stress) for the two cases plotted against EN1993-1-9 detail category 160 for one year of continuous operation.

It was anticipated that the case 1 - half feed would result in a clearly worse fatigue life estimation. However, it should be noted that twice the amount of material has been processed in the second case. A second observation is that the relatively coarse and mono-sized feed population potentially leads to a relatively high stress amplitude in the full feed case. For future work it would be interesting to evaluate the relationship between feed size distribution and force, moment, power, and stress signal characteristics.

Conclusions

The results demonstrate that DEM with an advanced fracture model that simulates actual fracture of particles on large scale can be used to provide fatigue life estimations on mechanical parts in a crusher. The GPU implementation allows for computationally very effective implementation where the simulation time for this kind of problem has been reduced by orders of magnitude compared to previous commercial solutions.

In brief we may conclude:

- A new version of the fracture model presented by [7] and [8] has been integrated, verified and calibrated in Demify® with an HPC GPU implementation allowing for millions of elements.
- The simulation approach has been demonstrated on the cone crusher for two different feeding conditions.
- The resulting forces as calculated in the DEM has been used to demonstrate predicted fatigue failure life of the main shaft.

While this study is aimed at highlighting the potential, more work should be directed towards exploring e.g.:

- Include non-mono feed size distribution.
- Influence of size segregation in addition to misaligned feed.
- Influence of rock/ore strength properties.
- Integration with FEM for direct and accurate calculation of stresses in the mechanical system.
- Evaluate worn liner profiles.

The work on this paper demonstrates multidisciplinary approach and methodology that is capable of joining breakage simulations in DEM with calculation of the fatigue life of crusher components and thus the service life of the crusher. The importance of having proper feeding conditions in order to minimize the production costs in crushing can be demonstrated through simulation.

Finally, the critical next step is to compare the simulation results with new or available field experimental data for an even higher level of validation.

References

- [1] A. Gröndahl, G. Asbjörnsson, E. Hulthén och M. Evertsson, "Diagnostics of cone crusher feed segregation using power draw measurements," *Minerals Engineering*, vol. 127, pp. 15-21, 2018.
- [2] C. M. E. Johannes Quist, "Application of discrete element method for simulating feeding conditions and size reduction in cone crushers," i *XXV International Mineral Processing Congress (IMPC) 2010*, Brisbane, QLD, Australia/, 2010.
- [3] P. A. Cundall och O. D. L. Strack, "A discrete numerical model for granular assemblies," *Geotechnique*, vol. 29, pp. 47-65, 1979.
- [4] N. S. Weerasekara, M. S. Powell, P. W. Cleary, L. M. Tavares, M. Evertsson, R. D. Morrison, J. Quist och R. M. Carvalho, "The contribution of DEM to the science of comminution," *Powder Technology*, vol. 248, pp. 3-24, 2013.
- [5] D. O. Potyondy och P. A. Cundall, "A bonded-particle model for rock," *International Journal of Rock Mechanics and Mining Sciences*, vol. 41, pp. 1329-1364, 2004.
- [6] S. Ji, S. Sun och Y. Yan, "Discrete Element Modeling of Rock Materials with Dilated Polyhedral Elements," *Procedia Engineering*, vol. 102, pp. 1793-1802, 2015.
- [7] L. Liu och S. Ji, "Bond and fracture model in dilated polyhedral DEM and its application to simulate breakage of brittle materials," *Granular Matter*, vol. 21, p. 41, 5 2019.
- [8] G. Ma, W. Zhou och X.-L. Chang, "Modeling the particle breakage of rockfill materials with the cohesive crack model," *Computers and Geotechnics*, vol. 61, pp. 132-143, 2014.
- [9] G. Ma, W. Zhou, X.-L. Chang och M.-X. Chen, "A hybrid approach for modeling of breakable granular materials using combined finite-discrete element method," *Granular Matter*, vol. 18, p. 7, 2 2016.
- [10] J. Quist och C. M. Evertsson, "Cone crusher modelling and simulation using DEM," *Minerals Engineering*, vol. 85, pp. 92-105, 2016.
- [11] M. Johansson, J. Quist, M. Evertsson och E. Hulthén, "Cone crusher performance evaluation using DEM simulations and laboratory experiments for model validation," *Minerals Engineering*, Vol. %1 av %2103-104, pp. 93-101, 2017.
- [12] F. P. André och L. M. Tavares, "Simulating a laboratory-scale cone crusher in DEM using polyhedral particles," *Powder Technology*, vol. 372, pp. 362-371, 2020.
- [13] P. W. Cleary och R. D. Morrison, "Geometric analysis of cone crusher liner shape: Geometric measures, methods for their calculation and linkage to crusher behaviour," *Minerals Engineering*, vol. 160, p. 106701, 2021.

- [14] P. W. Cleary och M. D. Sinnott, "Simulation of particle flows and breakage in crushers using DEM: Part 1 – Compression crushers," *Minerals Engineering*, vol. 74, pp. 178-197, 2015.
- [15] A. Bilock, "A GPU Polyhedral Discrete Element Method - Formulation and implementation of large scale simulations for non-spherical particles using novel GPU techniques," Gothenburg, 2020.
- [16] European Union, "EN 1993-1-9 (2005) (English): Eurocode 3: Design of steel structures - Part 1-9: Fatigue," Authority: The European Union Per Regulation 305/2011, 2010.
- [17] ASTM, "Standard Practices for Cycle Counting in Fatigue Analysis E1049-85(2017)," 2017.
- [18] M. A. Miner, "Cumulative damage in fatigue," 1945.
- [19] A. Palmgren, "Durability of ball bearings," *ZVDI*, vol. 68, pp. 339-341, 1924.
- [20] L. F. Orozco, J.-Y. Delenne, P. Sornay och F. Radjai, "Discrete-element model for dynamic fracture of a single particle," *International Journal of Solids and Structures*, vol. 166, pp. 47-56, 2019.
- [21] E. Nematollahi, S. Zare, M. Maleki-Moghaddam, A. Ghasemi, F. Ghorbani och S. Banisi, "DEM-based design of feed chute to improve performance of cone crushers," *Minerals Engineering*, vol. 168, p. 106927, 2021.
- [22] G.-Y. Liu, W.-J. Xu, Q.-C. Sun och N. Govender, "Study on the particle breakage of ballast based on a GPU accelerated discrete element method," *Geoscience Frontiers*, vol. 11, pp. 461-471, 2020.
- [23] J. Lichter, K. Lim, A. Potapov och D. Kaja, "New developments in cone crusher performance optimization," *Minerals Engineering*, vol. 22, pp. 613-617, 2009.
- [24] H. Li, G. McDowell och I. Lowndes, "Discrete element modelling of a rock cone crusher," *Powder Technology*, vol. 263, pp. 151-158, 2014.
- [25] J. Eliáš, "Simulation of railway ballast using crushable polyhedral particles," *Powder Technology*, vol. 264, pp. 458-465, 2014.
- [26] G. W. Delaney, R. D. Morrison, M. D. Sinnott, S. Cummins och P. W. Cleary, "DEM modelling of non-spherical particle breakage and flow in an industrial scale cone crusher," *Minerals Engineering*, vol. 74, pp. 112-122, 2015.
- [27] R. A. Day och D. M. Potts, "Zero thickness interface elements—numerical stability and application," *International Journal for Numerical and Analytical Methods in Geomechanics*, vol. 18, pp. 689-708, 1994.
- [28] P. P. Camanho, C. G. Dávila och M. F. De Moura, "Numerical simulation of mixed-mode progressive delamination in composite materials," *Journal of Composite Materials*, vol. 37, p. 1415 – 1438, 2003.
- [29] M. L. Benzeggagh och M. Kenane, "Measurement of mixed-mode delamination fracture toughness of unidirectional glass/epoxy composites with mixed-mode bending apparatus," *Composites Science and Technology*, vol. 56, pp. 439-449, 1996.